

# Transport theory for electrical detection of the spin texture and spin-momentum locking of topological surface states

Shi-Han Zheng, Hou-Jian Duan, Mou Yang, and Rui-Qiang Wang<sup>1,\*</sup>

<sup>1</sup>*Guangdong Provincial Key Laboratory of Quantum Engineering and Quantum Material, ICMP and SPTE, South China Normal University, Guangzhou 510006, China*

(Dated: June 13, 2017)

The surface states of three-dimensional topological insulators exhibit a helical spin texture with spin locked to momentum. To date, however, the direct all-electrical detection of the helical spin texture has remained elusive owing to the lack of necessary spin-sensitive measurements. We here provide a general theory for spin polarized transports of helical Dirac electrons through spin-polarized scanning tunneling microscopy (STM). It is found that different from conventional magnetic materials, the tunneling conductance through the TI surface acquires an extra component determined by the in-plane spin texture, exclusively associated with spin momentum locking. Importantly, this extra conductance unconventionally depends on the spatial azimuthal angle of the magnetized STM tip, which is never carried out in previous STM theory. By magnetically doping to break the symmetry of rotation and time reversal of the TI surface, we find that the measurement of the spatial resolved conductance can reconstruct the helical structure of spin texture. Furthermore, one can extract the SML angle if the in-plane magnetization is induced purely by the spin-orbit coupling of surface Dirac electrons. Our theory offers an alternative way, rather than using angle resolved photoemission spectroscopy, to electrical identify the helical spin texture on TI surfaces.

The discovery of three-dimension topological insulators (TIs)<sup>1,2</sup>, such as Bi<sub>2</sub>Se<sub>3</sub> and Bi<sub>2</sub>Te<sub>3</sub>, has currently triggered great interest in surface electronics. The most striking hallmark of TIs is the gapless topological surface states, which exhibits a spin texture with the intrinsic spin of Dirac electrons locked to its momentum, thus protecting the Dirac electrons immune to the backscattering off perturbations with time reversal symmetry<sup>3-5</sup>. This spin-momentum locking (SML) nature provides a concept for electrical manipulation of spin in a controlled fashion and makes TI particularly promising for spintronic devices and topological quantum computation<sup>6-8</sup>. Though such spin helicity has been experimentally observed by spin-resolved angle resolved photoemission spectroscopy (ARPES)<sup>9-12</sup> or polarized optical spectroscopic techniques<sup>13</sup>, it in present becomes extremely desirable to all-electrically detect the unique SML nature and resulting spin texture from electron transports. Theoretically, two-terminal spin valve<sup>14,15</sup> and three-terminal asymmetric structure<sup>16-18</sup> have been suggested to extract the information of SML by probing the spin-polarized currents along TI surface. In realistic experiments<sup>19-22</sup>, however, it remains great challenging due to unavoidable disturbance from bulk states<sup>23</sup>.

Alternatively, the imaging of scanning tunneling microscopy (STM) serves as a powerful tool to probe the nature of topological surface states by analyzing the quasi-particle interference (QPI) in Fourier-transform scanning-tunneling spectroscopy<sup>4,23-29</sup>, caused by scattering off impurities on the TI surface. The SML nature is manifested indirectly by the absence of backscattering between states of opposite momentum and opposite spin. Nevertheless, these QPI patterns do not show any signature of magnetic scattering even if the forbidden backscattering is lifted since the QPI reveals only the spin-conserving scattering. To extract the fingerprint of spin texture, the measurement of magnetization patterns with spin-polarized STM was suggested<sup>23,29-32</sup>. One, however, can note that most experiments only focus on the probing of the out-of-plane spin texture<sup>33,34</sup> while the in-plane spin texture, vital

for understand the SML nature, receives no attention due to complex physics in TIs. According to theory<sup>35-37</sup>, the spin-resolved STM conductance  $dI/dV$  links to the magnetization of tip and sample through

$$dI(\mathbf{r})/dV \propto \rho_t \rho(\mathbf{r}, eV) + |\mathbf{m}_t| |\mathbf{M}(\mathbf{r}, eV)| \cos \theta. \quad (1)$$

Here,  $\rho_t[\rho(\mathbf{r}, eV)]$  and  $\mathbf{m}_t[\mathbf{M}(\mathbf{r}, eV)]$  are, respectively, the charge and magnetization density of tip (substrate), and  $\theta$  is the angle between the tip and sample magnetization. In Eq. (1), if polarizing the substrate  $\mathbf{M}(\mathbf{r}, eV) = M_z(\mathbf{r}, eV)\hat{z}$  along z-direction, perpendicular to the surface, the conductance is proportional only to the polar angle  $\theta_t$  of tip magnetization, but independent of its azimuthal angle  $\varphi_t$ . The situation, however, is radically changed if the substrate is the polarized TIs since the spin polarization  $M_z(\mathbf{r}, eV)$  can induce the extra in-plane components  $\mathbf{M}_{\parallel}(\mathbf{r}, eV) = (M_x(\mathbf{r}, eV), M_y(\mathbf{r}, eV))$  due to strong spin-orbit interactions<sup>38,39</sup>. As a consequence, the total magnetization distorts from the primary z-axis and contributes an extra component of conductance. In this paper, we get insight into this new physics and modify the formula (1) to be suitable for the helical topological surface. It is found that the conductance is dependent on the azimuthal angle of tip magnetization, which has no analog in conventional magnetic metal, from which one can electrically probe the in-plane spin texture in real space and further to extract the SML angle of pristine topological states.

*Formulas for spin-polarized transports*— To connect  $\mathbf{M}_{\parallel}(\mathbf{r}, eV)$  to conductance, we employ a typical experimental setup as shown in Fig. 1, where a spin-polarized STM tip is placed over a host surface of TIs, absorbed by a magnetic impurity whose position is chosen as the original point ( $\mathbf{r} = 0$ ). The introduction of magnetic impurity has three-fold meanings: (1) Polarizing the topological surface. Although the topological surface states have a specific spin orientation in momentum space, they have no net polarization in real space due to the presence of time-reversal symmetry;

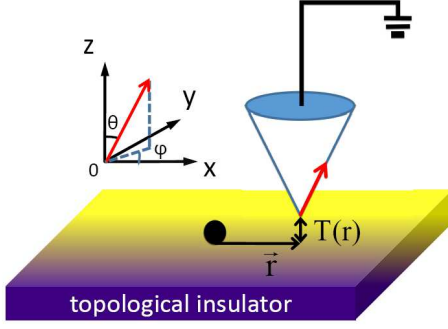


FIG. 1. (Color online) Schematic representation of the proposed experimental setup. The polar ( $\theta_t$ ) and the azimuthal angles ( $\varphi_t$ ) of the tip magnetization  $\mathbf{m}_t$  are shown. All the in-plane angles are measured with respect to the direction of x axis anticlockwise.  $\mathbf{r}$  is in-plane vector of tip position measured from impurity point and  $T(\mathbf{r})$  denotes the tip-surface coupling.

(2) Inducing the planar magnetism  $\mathbf{M}_{||}(\mathbf{r}, eV)$  and (3) generating  $\varphi_t$ -dependent current. The points (2) and (3) are based on breaking of the spatial rotate symmetry by the impurity. For undoped surface, the in-plane magnetism and  $\varphi_t$ -dependent current must vanish when integrating over the momentum. We model the Hamiltonian of the spin-polarized STM tip as  $H_{tip} = \sum_{\mathbf{k}} c_{\mathbf{k}}^\dagger [\epsilon_{\mathbf{k}} + \mathbf{m}_t \cdot \boldsymbol{\sigma}] c_{\mathbf{k}}$ , with  $\mathbf{m}_t$  the magnetization vector and  $\boldsymbol{\sigma}$  the vector of spin Pauli matrices, and the hybridized Hamiltonian between tip and topological surface as  $H_{hyb} = \int \int d\mathbf{r}_1 d\mathbf{r}_2 \psi_t^\dagger(\mathbf{r}_1, t) T(\mathbf{r}_1, \mathbf{r}_2) \psi_s(\mathbf{r}_2, t) + h.c.$ , where the quantum field operators  $\psi_\eta(\mathbf{r}, t) = \frac{1}{\sqrt{N}} \sum_{\mathbf{k}} c_{\eta\mathbf{k}}^\dagger(t) e^{-i\mathbf{k} \cdot \mathbf{r}}$  with  $c_{\eta\mathbf{k}}^\dagger(t) = (c_{\eta\mathbf{k}\uparrow}^\dagger(t), c_{\eta\mathbf{k}\downarrow}^\dagger(t))$  is the creation operator of electrons for surface ( $\eta = s$ ) and tip ( $\eta = t$ ). We choose the spin-quantization axis of the surface electrons as the global reference axis. The tip-surface coupling is assumed to be spin independent  $T(\mathbf{r}_1, \mathbf{r}_2) = T_0(\mathbf{r}_1) \delta(\mathbf{r}_2 - \mathbf{r})$  with  $\mathbf{r}$  being the in-plane spatial vector of tip measured from the impurity point. Here, the coupling between the tip and impurity is neglected due to weak interaction since we focus on large  $\mathbf{r}$ . By introduction of unitary matrix

$$U = \begin{bmatrix} \cos(\theta_t/2) e^{-i\varphi_t} & -\sin(\theta_t/2) e^{-i\varphi_t} \\ \sin(\theta_t/2) & \cos(\theta_t/2) \end{bmatrix}, \quad (2)$$

where  $\theta_t(\varphi_t)$  is the polar (azimuthal) angle of the tip magnetization  $\mathbf{m}_t$ , one can diagonalize  $H_{tip} = \sum_{\mathbf{k}\alpha} (\epsilon_{\mathbf{k}} + \alpha |\mathbf{m}_t|) \gamma_{t,\mathbf{k}\alpha}^\dagger \gamma_{t,\mathbf{k}\alpha}$ . Here, the quasi-particle operator  $(\gamma_{t,\mathbf{k}+}, \gamma_{t,\mathbf{k}-}) = U^\dagger (c_{\mathbf{k}\uparrow}, c_{\mathbf{k}\downarrow})$  with  $\alpha = \pm$  parallel (antiparallel) to tip magnetization. In this basis, the spin flipping due to noncollinear arrangement between the magnetic moments of the substrate and tip enters the tip-surface tunneling, which is rewritten as

$$H_{hyb} = \int \int d\mathbf{r}_1 d\mathbf{r}_2 \psi_t^\dagger(\mathbf{r}_1, t) \tilde{T}(\mathbf{r}_1, \mathbf{r}_2) \gamma_t(\mathbf{r}_2, t) + h.c., \quad (3)$$

where the renormalized coupling matrix  $\tilde{T}(\mathbf{r}_1, \mathbf{r}_2) = T(\mathbf{r}_1, \mathbf{r}_2) U^{-1}$  has nondiagonal term in spin space. The current through the tip is calculated with  $I = -e \frac{\partial}{\partial t} \sum_{\alpha} \int d\mathbf{r}_1 \times$

$\langle \Psi_t^{\alpha\dagger}(\mathbf{r}_1, t) \Psi_t^{\alpha}(\mathbf{r}_1, t) \rangle$ . Carrying out the equation of motion for non-equilibrium Green's function on the Keldysh technique, we obtain the conductance as (see the Supplementary Methods)

$$I = -2e |T_0|^2 \sum_{\mathbf{p}} \int \frac{d\omega}{2\pi} \times Tr \{ \text{Re}[g^r(\mathbf{r}, \mathbf{r}, \omega) U g_{\mathbf{p}}^<(\omega) U^{-1} + g^<(\mathbf{r}, \mathbf{r}, \omega) U g_{\mathbf{p}}^a(\omega) U^{-1}] \}, \quad (4)$$

where  $g^{r(<)}(\mathbf{r}, \mathbf{r}; \omega)$  is the retarded (lesser) Green's function of topological surface states in real-frequency space and  $g_{\mathbf{p}}^{a(<)}(\omega)$  is the advanced (lesser) Green's function of tip in momentum-frequency space. We denote  $T_0 = \int d\mathbf{r}' e^{-i\mathbf{p} \cdot \mathbf{r}'} T_0(\mathbf{r}')$  assumed independence of momentum. Compared to previous derivation<sup>40–42</sup>, an important difference is the matrix  $g^r(\mathbf{r}, \mathbf{r}; \omega)$  including the spin flipping when Dirac electrons travel on the topological surface.

As usual, we define the charge density of TIs as  $\rho(\mathbf{r}, \omega) = -\frac{1}{2\pi} \text{Im} \text{Tr}[g(\mathbf{r}, \mathbf{r}, \omega + i0^+)]$  and its spin texture as  $\mathbf{M}(\mathbf{r}, \omega) = -\frac{1}{2\pi} \text{Im} \text{Tr}[\frac{\boldsymbol{\sigma}}{2} g(\mathbf{r}, \mathbf{r}, \omega + i0^+)]$ . Finally, we in the zero-temperature limit obtain the expression for conductance at bias  $eV$ , which can be divided to two parties  $G(\mathbf{r}) = G_0(\mathbf{r}) + G_{flip}(\mathbf{r})$ , with

$$G_0(\mathbf{r}) = \pi e |T_0|^2 [\rho(\mathbf{r}, eV) \rho_t + M_z(\mathbf{r}, eV) |\mathbf{m}_t| \cos \theta_t], \quad (5)$$

$$G_{flip}(\mathbf{r}) = \pi e |T_0|^2 |\mathbf{m}_t| |\mathbf{M}_{||}(\mathbf{r}, eV)| \times \sin \theta_t \cos(\varphi_t - \varphi_{\mathbf{M}}), \quad (6)$$

where  $\varphi_{\mathbf{M}}$  is the azimuthal angle of  $\mathbf{M}(\mathbf{r}, eV)$ . The conductance  $G_0(\mathbf{r})$  recovers the usual formula in Eq. (1), which is azimuthal independent. The most interest is  $G_{flip}(\mathbf{r})$  in Eq. (6), which is contributed by spin-flipping process contained in Green's function  $g_{\sigma\bar{\sigma}}^r(\mathbf{r}, \mathbf{r}, \omega)$  when an electron is scattered off the magnetic impurity. Importantly, such dependence of the tunneling conductance on the azimuthal angle of the tip magnetization has no analog in conventional magnetic metals.

*Probing of spin texture in linear dispersion*— In this section, we will demonstrate that how the measurement of  $G_{flip}(\mathbf{r})$  with a spin-polarized STM reconstructs the spin texture of the TI surface states and then further determines its SML angle in the real space. It is easy to verify that the presence of magnetic impurities is strictly necessary since  $M_{||}(\mathbf{r}, eV)$  vanishes without the magnetic impurity.

To calculate  $\mathbf{M}_{||}(\mathbf{r}, eV)$  in Eq. (6), we must first obtain the dirtied Green's function of Dirac electrons  $g(\mathbf{r}, \mathbf{r}, \omega)$ , which can be calculated with T-matrix approach<sup>43–45</sup>.

$$g(\mathbf{r}, \mathbf{r}, \omega) = g_0(0, \omega) + g_0(\mathbf{r}, \omega) T(\omega) g_0(-\mathbf{r}, \omega), \quad (7)$$

which takes into account the multiple scattering events of electrons by the impurity. Here, the impurity-free Green's function  $g_0(\mathbf{r}, \omega)$  is the Fourier transform of  $g_0(\mathbf{k}, \omega) =$

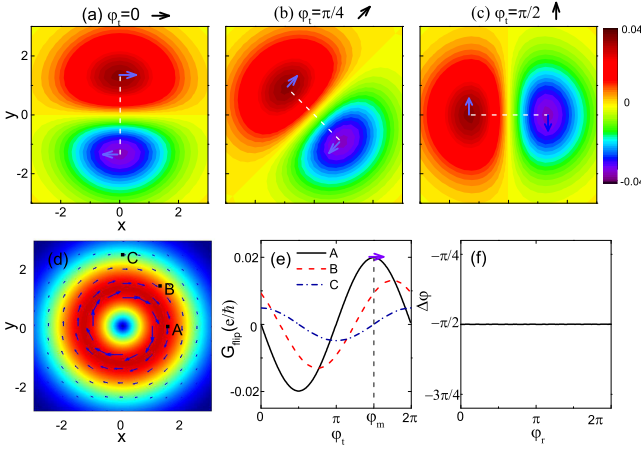


FIG. 2. (Color online) (a)-(c) Spatially resolved conductance maps for different directions of tip magnetization  $\varphi_t = 0, \pi/4, \pi/2$  with  $\theta_t = \pi/2$  and  $eV = 0.2$ . (d) The distribution of in-plane spin texture  $\mathbf{M}_{||}(\mathbf{r}, eV)$  with arrows showing the directions and the color code representing the degree of the spin polarization. (e) Dependence of  $G_{flip}(\mathbf{r})$  on  $\varphi_t$  for three points A( $r = 1.5$  and  $\varphi = 0$ ), B( $r = 2$  and  $\varphi = \pi/4$ ), and C( $r = 2.5$  and  $\varphi = \pi/2$ ) indicated in (d). (f) Direction difference  $\Delta\varphi = |\varphi_r - \varphi_M|$  between  $\mathbf{r}$  and  $\mathbf{M}_{||}(\mathbf{r}, eV)$  as a function of spatial direction  $\varphi_r$  for  $r = 2$ . The chosen other parameters are  $D_c = 1.5$ ,  $\hbar = 1$ ,  $v_f = 1$ ,  $U_0 = 0$ ,  $U_z = 100$ ,  $|\mathbf{m}_t| = 0.5$ ,  $\rho_t = 1$ , and  $T_0 = 1$  for all diagrams.

$[\omega + i0^+ - H_{TI}^0]^{-1}$  with respect to the bare TI Hamiltonian  $H_{TI}^0$ , and the T-matrix is given by the Bethe-Scalpeter equation  $T(\omega) = V[1 - Vg_0(0, \omega)]^{-1}$ . The impurity potential is assumed in the form of  $V = (U_0 - U_z\sigma_z)$ , consisting of a scalar potential  $U_0$  and a magnetic potential  $U_z$  polarized perpendicular to the surface. The Hamiltonian of surface of TIs is described by

$$H_{TI}^0(\lambda) = \sum_{\mathbf{k}} [\hbar v_f(\sigma \times \mathbf{k})_z + \frac{\lambda}{2}(k_+^2 + k_-^2)\sigma_z], \quad (8)$$

which includes the warping term with strength  $\lambda$  and  $k_{\pm} = k_x \pm ik_y$ .

We first consider the case of  $\lambda = 0$  and plot the real-space distribution of the in-plane spin texture  $\mathbf{M}_{||}(\mathbf{r}, eV)$  in Fig. 2(d) and of the spin-flipping conductance  $G_{flip}(\mathbf{r})$  in Figs. 2(a)-(c) for different azimuthal angles  $\varphi_t$  of the polarized tip. For a fixed tip direction  $\varphi_t$ ,  $G_{flip}(\mathbf{r})$  is spatial asymmetry, with the extremum in a circle around the original point appearing along certain radius (dashed white line). The positive and negative maxima, respectively, correspond to the in-plane magnetization  $\mathbf{M}_{||}(\mathbf{r}, eV)$  parallel and antiparallel to the polarized direction of the STM tip, as indicated by arrows, due to spin selection of the tip. As one rotates the tip direction  $\varphi_t = 0, \pi/4, \pi/2$ , the extremum position also rotates anticlockwise with the unchanged magnitude, indicating the in-plane magnetization  $\mathbf{M}_{||}(\mathbf{r}, eV)$  tangential to the concentric circle with clockwise helicity. To accurately determine the orientation of  $\mathbf{M}_{||}(\mathbf{r}, eV)$ , we depict the dependence of  $G_{flip}(\mathbf{r})$  on  $\varphi_t$  in Fig. 2(e), where the position of peak just corresponds to  $\varphi_M$ . By choosing any different positions, e.g.,

points A, B, and C indicated in Fig. 2(d), it is found that the direction between  $\mathbf{r}$  and  $\mathbf{M}_{||}(\mathbf{r}, eV)$  always satisfies a relation  $\Delta\varphi = |\varphi_r - \varphi_M| = \pi/2$ , where  $\varphi_r$  is the azimuthal angle of  $\mathbf{r}$ , as shown in Fig. 2(f). Therefore, the measurement of  $G_{flip}(\mathbf{r})$  can ascertain the in-plane spin texture in Fig. 2(d). To understand the origin of relation  $|\varphi_r - \varphi_M| = \pi/2$ , we further derive the analytical formula with  $H_{TI}^0(\lambda = 0)$ , from which  $g_0(0, \omega) = \frac{1}{4(\hbar v_f)^2} [\frac{\omega}{\pi} \ln(\frac{\omega^2}{D_c^2 - \omega^2}) - i|\omega| \Theta(D_c - |\omega|)]$  and

$$g_0(\mathbf{r}, \omega) = -\frac{\omega}{2\pi v_f^2} \begin{pmatrix} K_0(\xi) & e^{-i\varphi_r} K_1(\xi) \\ e^{i\varphi_r} K_1(\xi) & K_0(\xi) \end{pmatrix}. \quad (9)$$

Here,  $D_c$  is the cutoff energy for the band width of surface states,  $\xi = -i|\mathbf{r}|\omega/\hbar v_f$ , and  $K_n(x)$  is the Bessel functions of the  $n$ th-order.  $\varphi_r$  in Eq. (9) arises from the Fourier transform of momentum direction  $\varphi_{\mathbf{k}}$ . Finally, we obtain azimuthal angle of the in-plane magnetization

$$\cos \varphi_M = M_x / \sqrt{M_x^2 + M_y^2} = \sin \varphi_r, \quad (10)$$

and its magnitude  $|\mathbf{M}_{||}(\mathbf{r}, eV)| = \frac{\omega^2 U_z}{A\pi^3 v_f^2} K_0(\xi) K_1(\xi)$  with  $A = 1 - 2g_0(0, \omega)U_0 - g_0(0, \omega)^2(U_z^2 - U_0^2)$ . Thus, we obtain  $|\varphi_M - \varphi_r| = \pi/2$ , which is corresponding to SML angle  $|\varphi_M - \varphi_{\mathbf{k}}| = \pi/2$  of the pristine TI in momentum space. Notice that though the in-plane magnetization in real space is induced by the impurity magnetism, it also stems purely from the spin-orbit effect. Consequently, the planar  $\mathbf{M}_{||}(\mathbf{r}, eV)$  still contains the information of SML, reflected by the spin-position locking.

With Eq. (10), we can further rewrite Eq. (6) as

$$\mathbf{M}_{||}(\mathbf{r}, eV) = |\mathbf{M}_{||}(\mathbf{r}, eV)| \hat{\mathbf{r}} \times \hat{U}_z, \quad (11)$$

where  $\hat{U}_z$  is the unit vector along  $z$  direction. Obviously,  $\mathbf{M}_{||}(\mathbf{r}, eV)$  is perpendicular to  $\mathbf{r}$ , which is a consequence of the Dzyaloshinskii-Moriya interaction caused by the helical spin structure of Dirac surface states on TIs. Therefore, the measurement of  $\mathbf{M}_{||}(\mathbf{r}, eV)$  not only provides a way to extract the pristine SML angle, but also the strength of the DM interaction. In addition, here due to  $G_{flip}(\mathbf{r}) \propto \cos(\varphi_t - \varphi_r + \pi/2)$ , rotating the tip has equal role with the rotation of spatial position around the impurity, which is helpful in realistic measurement.

As for the magnitude of  $\mathbf{M}_{||}(\mathbf{r}, eV)$  at certain point  $\mathbf{r}$ , we can determine it by rotation of tip direction, namely,  $|\mathbf{M}_{||}(\mathbf{r}, eV)| = \text{Max}[G_{flip}(\mathbf{r}, \varphi_t)] - \text{Min}[G_{flip}(\mathbf{r}, \varphi'_t)]/B$  with  $B = 2\pi e|T_0|^2|\mathbf{m}_t|$ .

*Probing of spin texture in warping dispersion*—For  $\lambda \neq 0$ , the magnetization density  $\mathbf{M}_{||}(\mathbf{r}, eV)$  is demonstrated in Fig. 3(d). Compared to Fig. 2(d), introduction of the warping term greatly modifies the surface magnetism, i.e., not only modifying  $M_z(\mathbf{r}, eV)$  but also making  $\mathbf{M}_{||}(\mathbf{r}, eV)$  deviate from the circular structure or  $|\varphi_M - \varphi_r| \neq \pi/2$ . Especially, for large distance  $|\mathbf{r}|$ , there appear three new circular centers with anticlockwise helical spin structure, exhibiting  $C_3$  symmetry of lattice structure describing by the TI Hamiltonian in Eq. (8). A main reason for large change of the spin texture is that the warping term generates additional in-plane magnetization  $M_r(\mathbf{r}, eV)$  along radial direction(or  $\mathbf{r}$ ). The component

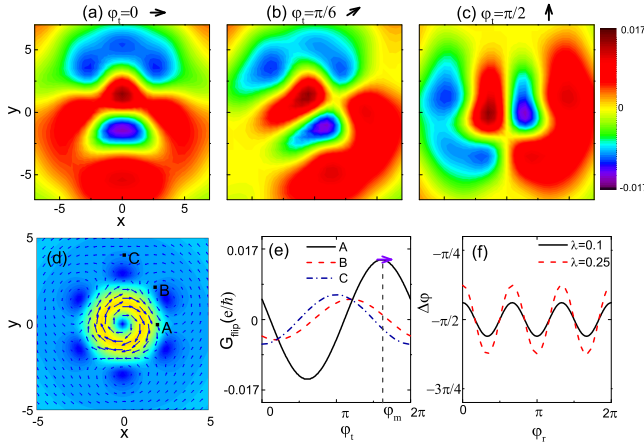


FIG. 3. (Color online) (a)-(c) Spatially resolved conductance in warping dispersion  $\lambda = 0.25$  maps for different directions of tip magnetization  $\varphi_t = 0, \pi/6, \pi/2$  with  $eV = 0.6$ . (d) The distribution of in-plane spin texture  $\mathbf{M}_{\parallel}(\mathbf{r}, eV)$  with arrows showing the directions and the color code representing the degree of the spin polarization. (e) Dependence of  $G_{flip}(\mathbf{r})$  on  $\varphi_t$  for three points A ( $r = 2$  and  $\varphi = 0$ ), B ( $r = 3$  and  $\varphi = \pi/4$ ), and C ( $r = 4$  and  $\varphi = \pi/2$ ) indicated in (d). (f) Direction difference  $\Delta\varphi$  as a function of spatial direction  $\varphi_r$  for  $r = 2$ . The rest of parameters refer to data used above.

$M_r(\mathbf{r}, eV)$  is attributed to the antiferromagnetic Ruderman-Kittel-Kasuya-Yosida interaction along the line joining the impurities<sup>39</sup>. In this situation,  $\mathbf{M}_{\parallel}(\mathbf{r}, eV)$  has a complex dependence on the spatial direction. When we scan the tip over the whole surface with fixed tip azimuthal angle, e.g.,  $\varphi_t = 0$  in Fig. 3(a), the alternating positive and negative maxima of conductance along radial direction reflect the alternating change of spin structure in Fig. 3(e). With the tip rotating from Figs. 3(a) to (c), the extremum also rotates anticlockwise. Unlike the case without warping term in Figs. 2(a)-(c), the structure of extremum regime from Figs. 3(a) to (c) is changed, indicating the spin texture deviating from the concentric circle. Even so, we still can exactly determine the direction of magnetization at arbitrary point only by rotating the tip direction around the  $z$  axis. For example, to determine the direction  $\varphi_M$  of magnetization in points A, B, and C labeled in Fig. 3(d), one can plot  $G_{flip}(\mathbf{r})$  vs  $\varphi_t$  as shown in Fig. 3(e).  $\varphi_M$  is equal to the size of  $\varphi_t$  at the conductance peak.

From discussions in Fig. 2, we are known that the direction difference  $\Delta\varphi = |\varphi_r - \varphi_M|$  between  $\mathbf{r}$  and  $\mathbf{M}_{\parallel}(\mathbf{r}, eV)$  can characterize the SML angle well. In Fig. 3(f), we depict  $\Delta\varphi$  as a function of  $\varphi_r$  in order to clarify the effect of warping term. As the warping term is added,  $\Delta\varphi$  deviates from the perfect SML ( $\Delta\varphi = \pi/2$ ) and exhibits an oscillating behavior. With the increase of  $\lambda$ , the deviation amplitude becomes larger and larger but at the same time the oscillating period of  $2\pi/3$  remains unchanged, reappearing the  $C_3$  symmetry of hexagonal lattice in Fig. 3(d). The change of  $\varphi_M$  is remarkable along directions of  $\varphi_r = n\pi/3$  with  $n = 0, 1, 2, 3, 4, 5$  due to the strong out-of-plane magnetization, which corresponds to the center of the sides of the hexagon of the Fermi surface. By contrast, for  $\varphi_r = n\pi/6$  with  $n = 1, 3, 5, 7, 9, 11$  corresponding to the

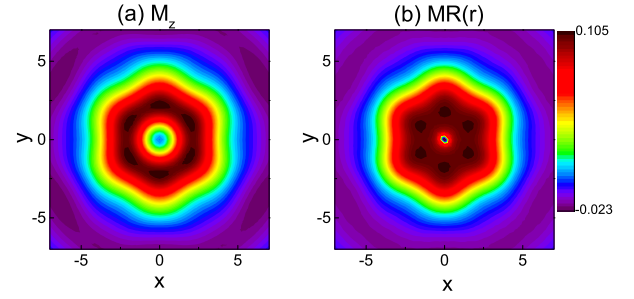


FIG. 4. (Color online) Spatially resolved out-of-plane spin texture  $M_z(\mathbf{r}, eV)$  (a) and magnetoresistance  $MR$  map (b) with the color code representing the magnitude. The directions of tip magnetization is  $\theta_t = 0$  with  $eV = 0.6$ . And strength of warp term is  $\lambda = 1$ . The rest of parameters refer to data used above.

corners of the hexagonal pattern, the pristine perfect SML angle  $\Delta\varphi = \pi/2$  (or  $\mathbf{M}_{\parallel}(\mathbf{r}, eV) \perp \mathbf{r}$ ) is still abided by due to the vanishing out-of-plane magnetization.

An important feature for the TI with warping term is the staggered structure of the out-of-plane magnetization  $M_z(\mathbf{r}, eV)$  as shown in Fig. 4(a), where alternating positive and negative values have six symmetric regions. To probe its complex spin texture, we can set  $\theta_t = 0$  and so the total conductance is  $G_0(\mathbf{r})$ , whose spin dependence of  $G_0(\mathbf{r})$  stems completely from the  $M_z(\mathbf{r}, eV)$ . In this case, we keep the spin-polarized STM magnetization either parallel or antiparallel to the  $z$  axis to define the magnetoresistance (MR) effect, given by

$$MR(\mathbf{r}) = \frac{G_0(\mathbf{r}, \varphi_t = 0) - G_0(\mathbf{r}, \varphi_t = \pi)}{G_0(\mathbf{r}, \varphi_t = 0) + G_0(\mathbf{r}, \varphi_t = \pi)}. \quad (12)$$

We depict  $MR(\mathbf{r})$  in Fig. 4(b), which exhibits six regions with alternating high and low conductance density, completely constituting the spatial pattern of spin texture  $M_z(\mathbf{r}, eV)$  in Figs. 4(a).

**Conclusions**— In conclusion, employing the nonequilibrium Green's function, we present a general theory for spin polarized transports of Dirac electrons through a spin-polarized STM. In order to extract quantitative information about spin texture, we need to break the symmetry of rotation and time reversal with a typical impurity model. It is found that the conductance is modified by an extra component exclusively associated with in  $xy$ -plane spin texture, which exhibits an unconventional dependence on the azimuthal angle of the tip magnetization. The analysis of azimuthal angle dependent conductance provides a direct method of measurement of the local in-plane spin texture of the Dirac electrons on the surface. By measurement of the spatial resolved conductance  $G_{flip}(\mathbf{r})$ , we can not only reconstruct the helical structure of spin texture but also can extract the SML angle if the in-plane magnetization is induced purely by the spin-orbit coupling of the surface Dirac election. Experimentally, the magnetic tip can be prepared by coating antiferromagnetic Cr on tungsten tips where the magnetic direction of the tip can be controlled by the Cr thickness, either in plane ( $> 30\text{nm}$ ) or out of plane ( $\sim 5\text{nm}$ )<sup>37,46</sup>. Therefore, the measurement of the in-plane

magnetization offers an alternative way to identify the topology nature on TI surfaces.

- 
- \* rqwanggz@163.com
- <sup>1</sup> Chen, Y. L. *et al.* Experimental Realization of a Three-Dimensional Topological Insulator, Bi<sub>2</sub>Te<sub>3</sub>. *Science* **325**, 178 (2009).
  - <sup>2</sup> Zhang, H., Liu, C.-X., Qi, X.-L., Dai, X., Fang, Z., & Zhang, S.-C. Topological insulators in Bi<sub>2</sub>Se<sub>3</sub>, Bi<sub>2</sub>Te<sub>3</sub> and Sb<sub>2</sub>Te<sub>3</sub> with a single Dirac cone on the surface. *Nat. Phys.* **5**, 438 (2009).
  - <sup>3</sup> Qi, X.L. & Zhang, S C. Topological insulators and superconductors. *Rev. Mod. Phys.* **83**, 1057 (2011).
  - <sup>4</sup> Roushan, P. *et al.* Topological surface states protected from backscattering by chiral spin texture. *Nature* **460**, 1106 (2009).
  - <sup>5</sup> Beidenkopf, H. *et al.* Spatial Fluctuations of Helical Dirac Fermions on the Surface of Topological Insulators. *Nat. Phys.* **7**, 939 (2011).
  - <sup>6</sup> Hasan, M. Z. & Kane, C. L. Colloquium: Topological insulators. *Rev. Mod. Phys.* **82**, 3045 (2010).
  - <sup>7</sup> Pesin, D. & MacDonald, A. H. Spintronics and pseudospintronics in graphene and topological insulators. *Nat. Mater.* **11**, 409–416 (2012).
  - <sup>8</sup> Fu, L., Kane, C. L., & Mele, E. J. Topological Insulators in Three Dimensions. *Phys. Rev. Lett.* **98**, 106803 (2007).
  - <sup>9</sup> Hsieh, D. *et al.* Observation of Unconventional Quantum Spin Textures in Topological Insulators. *Science* **323**, 919 (2009).
  - <sup>10</sup> Xia, Y. *et al.* Observation of a large-gap topological-insulator class with a single Dirac cone on the surface. *Nat. Phys.* **5**, 398 (2009).
  - <sup>11</sup> Hsieh, D. *et al.* A tunable topological insulator in the spin helical Dirac transport regime. *Nature* **460**, 1101 (2009).
  - <sup>12</sup> Xu, S. Y. *et al.* Hedgehog spin texture and Berry's phase tuning in a magnetic topological insulator. *Nat. Phys.* **8**, 616 (2012).
  - <sup>13</sup> McIver, J. W. *et al.* Control over topological insulator photocurrents with light polarization. *Nat. Nanotechnol.* **7**, 96–100 (2012).
  - <sup>14</sup> Yokoyama, T. *et al.* Anomalous magnetoresistance of a two-dimensional ferromagnet/ferromagnet junction on the surface of a topological insulator. *Phys. Rev. B* **81**, 121401 (2010).
  - <sup>15</sup> Taguchi, K. *et al.* Giant magnetoresistance in the junction of two ferromagnets on the surface of diffusive topological insulators. *Phys. Rev. B* **89**, 085407 (2014).
  - <sup>16</sup> Roy, S., Soori, A., & Das, S. Tunnel magnetoresistance scan of a pristine three-dimensional topological insulator. *Phys. Rev. B* **91**, 041109 (2015).
  - <sup>17</sup> Roy, S., Saha, K., & Das, S. Probing surface states exposed by crystal terminations at arbitrary orientations of three-dimensional topological insulators. *Phys. Rev. B* **91**, 195415 (2015).
  - <sup>18</sup> Roy, S. & Das, S. Transport signatures of surface potentials on three-dimensional topological insulators. *Phys. Rev. B* **93**, 085422 (2016).
  - <sup>19</sup> Dankert, A. *et al.* Room Temperature Electrical Detection of Spin Polarized Currents in Topological Insulators. *Nano Lett.* **15**, 7976 (2015).
  - <sup>20</sup> Liu, L. *et al.* Spin-polarized tunneling study of spin-momentum locking in topological insulators. *Phys. Rev. B* **91**, 235437 (2015).
  - <sup>21</sup> Tian, J. *et al.* Electrical injection and detection of spin-polarized currents in topological insulator Bi<sub>2</sub>Te<sub>2</sub>Se. *Scientific Reports* **5**, 14293 (2015).
  - <sup>22</sup> Li, C. H. *et al.* Electrical detection of charge-current-induced spin polarization due to spin-momentum locking in Bi<sub>2</sub>Se<sub>3</sub>. *Nat. Nanotechnol.* **9**, 218–224 (2014).
  - <sup>23</sup> Zhou, X. *et al.* Theory of quasiparticle scattering in a two-dimensional system of helical Dirac fermions: Surface band structure of a three-dimensional topological insulator. *Phys. Rev. B* **80**, 245317 (2009).
  - <sup>24</sup> Oka, H. *et al.* Spin-polarized quantum confinement in nanostructures: Scanning tunneling microscopy. *Rev. Mod. Phys.* **86**, 1127 (2014).
  - <sup>25</sup> Song, C. L. *et al.* Probing Dirac Fermion Dynamics in Topological Insulator Bi<sub>2</sub>Se<sub>3</sub> Films with a Scanning Tunneling Microscope. *Phys. Rev. Lett.* **114**, 176602 (2015).
  - <sup>26</sup> Alpichshev, Z. *et al.* STM Imaging of Electronic Waves on the Surface of Bi<sub>2</sub>Te<sub>3</sub>: Topologically Protected Surface States and Hexagonal Warping Effects. *Phys. Rev. Lett.* **104**, 016401 (2010).
  - <sup>27</sup> Shunsuke, Y. *et al.* Scanning tunneling spectroscopy study of quasiparticle interference on the dual topological insulator Bi<sub>1-x</sub>Sb<sub>x</sub>. *Phys. Rev. B* **91**, 045423 (2015).
  - <sup>28</sup> Zhang, T. *et al.* Experimental Demonstration of Topological Surface States Protected by Time-Reversal Symmetry. *Phys. Rev. Lett.* **103**, 266803 (2009).
  - <sup>29</sup> Strðžeka, A. *et al.* Quasiparticle Interference around a Magnetic Impurity on a Surface with Strong Spin-Orbit Coupling. *Phys. Rev. Lett.* **107**, 186805 (2011).
  - <sup>30</sup> Kaladzhyan, V., Simon, P., & Bena, C. Determining the spin-orbit coupling via spin-polarized spectroscopy of magnetic impurities. *Phys. Rev. B* **94**, 134511 (2016).
  - <sup>31</sup> Wang, R.-Q., Zhong, M., Zheng, S.-H., Yang, M., & Wang, G.-H. Electrical manipulation of dynamic magnetic impurity and spin texture of helical Dirac fermions. *EPL* **114**, 37007 (2016).
  - <sup>32</sup> Liu, Q. *et al.* Magnetic Impurities on the Surface of a Topological Insulator. *Phys. Rev. Lett.* **102**, 156603 (2009).
  - <sup>33</sup> Yang, F. *et al.* Identifying Magnetic Anisotropy of the Topological Surface State of Cr<sub>0.05</sub>Sb<sub>1.95</sub>Te<sub>3</sub> with Spin-Polarized STM. *Phys. Rev. Lett.* **111**, 176802 (2013).
  - <sup>34</sup> Oka, H. *et al.* Spin-dependent quantum interference within a single magnetic nanos-structure. *Science* **327**, 843 (2010).
  - <sup>35</sup> Wortmann, D. *et al.* Resolving Complex Atomic-Scale Spin Structures by Spin-Polarized Scanning Tunneling Microscopy. *Phys. Rev. Lett.* **86**, 4132 (2001).
  - <sup>36</sup> Tersoff, J. & Hamann, D. R. Theory and Application for the Scanning Tunneling Microscope. *Phys. Rev. Lett.* **50**, 1998 (1983).
  - <sup>37</sup> Wiesendanger, R. Spin mapping at the nanoscale and atomic scale. *Rev. Mod. Phys.* **81**, 1495 (2009).
  - <sup>38</sup> Chirla, R. *et al.* Probing the Rashba effect via the induced magnetization around a Kondo impurity. *Phys. Rev. B* **87**, 245133 (2013).
  - <sup>39</sup> Biswas, R. R. & Balatsky, A. V. Impurity-induced states on the surface of three-dimensional topological insulators. *Phys. Rev. B* **81**, 233405 (2010).
  - <sup>40</sup> Penteado, P. H. *et al.* Scanning tunneling microscope operating as a spin diode. *Phys. Rev. B* **84**, 125439 (2011).
  - <sup>41</sup> Fransson, J., Eriksson, O., & Balatsky, A. V. Theory of spin-polarized scanning tunneling microscopy applied to local spins. *Phys. Rev. B* **81**, 115454 (2010).
  - <sup>42</sup> Wang, R.Q. *et al.* Spin-dependent inelastic transport through single-molecule junctions with ferromagnetic electrodes. *Phys. Rev. B* **75**, 045318 (2007).
  - <sup>43</sup> Mahan, G. *Many-Particle Physics, Physics of Solids and Liquids* (Springer, 2000).
  - <sup>44</sup> Balatsky, A. V., Vekhter, I., & Zhu, J.-X. Impurity-induced states



in conventional and unconventional superconductors. *Rev. Mod. Phys.* **78**, 373 (2006).

- <sup>45</sup> Wang, R.Q., Sheng, L., Yang, M., Wang, B.G. & Xing, D. Y. Electrically tunable Dirac-point resonance induced by a nanomagnet absorbed on the topological insulator surface. *Phys. Rev. B* **91**, 245409 (2015).
- <sup>46</sup> Wachowiak, A. *et al.* *Science* **298**, 577 (2002).
- <sup>47</sup> Peng, H.L. *et al.* Aharonov-Bohm interference in topological insulator nanoribbons. *Nat. Material.* **9**, 225 (2010).

## I. ACKNOWLEDGMENTS

This work was supported by National Natural Science Foundation of China (Grant Nos. 11474106 and 11274124), and by the Innovation Project of Graduate School of South China Normal University.

## II. AUTHORS CONTRIBUTIONS

R.Q.W. conceived the idea. S.H.Z. performed the calculation and provided all of the figures. R.Q.W. and S.H.Z. contributed to the interpretation of the results and wrote the manuscript. H.J.D. and M.Y. joined in the data analysis and contributed in the discussion. All authors reviewed the manuscript.

## III. ADDITIONAL INFORMATION

**Competing financial interests:** The authors declare no competing financial interests.

**Figure legends** Fig.1: Schematic representation of the proposed experimental setup. The polar ( $\theta_t$ ) and the azimuthal

angles( $\varphi_t$ ) of the tip magnetization  $\mathbf{m}_t$  are shown. All the in-plane angles are measured with respect to the direction of x axis anticlockwise.  $\mathbf{r}$  is in-plane vector of tip position measured from impurity point and  $T(\mathbf{r})$  denotes the tip-surface coupling.

Fig.2: (a)-(c) Spatially resolved conductance maps for different directions of tip magnetization  $\varphi_t = 0, \pi/4, \pi/2$  with  $\theta_t = \pi/2$  and  $eV = 0.2$ . (d) The distribution of in-plane spin texture  $\mathbf{M}_{\parallel}(\mathbf{r}, eV)$  with arrows showing the directions and the color code representing the degree of the spin polarization. (e) Dependence of  $G_{flip}(\mathbf{r})$  on  $\varphi_t$  for three points A( $r = 1.5$  and  $\varphi = 0$ ), B( $r = 2$  and  $\varphi = \pi/4$ ), and C( $r = 2.5$  and  $\varphi = \pi/2$ ) indicated in (d). (f) Direction difference  $\Delta\varphi = |\varphi_{\mathbf{r}} - \varphi_{\mathbf{M}}|$  between  $\mathbf{r}$  and  $\mathbf{M}_{\parallel}(\mathbf{r}, eV)$  as a function of spatial direction  $\varphi_{\mathbf{r}}$  for  $r = 2$ . The chosen other parameters are  $D_c = 1.5$ ,  $\hbar = 1$ ,  $v_f = 1$ ,  $U_0 = 0$ ,  $U_z = 100$ ,  $|\mathbf{m}_t| = 0.5$ ,  $\rho_t = 1$ , and  $T_0 = 1$  for all diagrams.

Fig.3: (a)-(c) Spatially resolved conductance in warping dispersion  $\lambda = 0.25$  maps for different directions of tip magnetization  $\varphi_t = 0, \pi/6, \pi/2$  with  $eV = 0.6$ . (d) The distribution of in-plane spin texture  $\mathbf{M}_{\parallel}(\mathbf{r}, eV)$  with arrows showing the directions and the color code representing the degree of the spin polarization. (e) Dependence of  $G_{flip}(\mathbf{r})$  on  $\varphi_t$  for three points A ( $r = 2$  and  $\varphi = 0$ ), B( $r = 3$  and  $\varphi = \pi/4$ ), and C( $r = 4$  and  $\varphi = \pi/2$ ) indicated in (d). (f) Direction difference  $\Delta\varphi$  as a function of spatial direction  $\varphi_{\mathbf{r}}$  for  $r = 2$ . The rest of parameters refer to data used above.

Fig.4: Spatially resolved out-of-plane spin texture  $\mathbf{M}_z(\mathbf{r}, eV)$  (a) and magnetoresistance  $MR$  map (b) with the color code representing the magnitude. The directions of tip magnetization is  $\theta_t = 0$  with  $eV = 0.6$ . And strength of warp term is  $\lambda = 1$ . The rest of parameters refer to data used above.